



# Microstructure and mechanical properties of laser-MIG hybrid multi-layer welded joints for 20-mm thick aluminum alloy plates

Zhibin Yang<sup>1</sup> · Likang Sheng<sup>1</sup> · Yanqi Xie<sup>1</sup>

Received: 17 November 2023 / Accepted: 8 April 2024 / Published online: 11 April 2024  
© International Institute of Welding 2024

## Abstract

Laser-MIG hybrid multi-layer welding was performed upon the 20-mm thick 6082-T6 aluminum alloy butt-joints. The weld formation, microstructure, and mechanical properties of the welded joints were studied in details. The results indicated that the well-formed weld without obvious incomplete fusion and cracks could be obtained by using the optimal welding parameters, only very few porosities appeared in the filling layer and covering layer. The equiaxed crystals and columnar crystals were respectively observed in the weld center and near the fusion in the weld metal; their sizes and widths of each layer were different. The microhardness values of the weld metal and heat-affected zone are lower than those of the base metal; the lowest microhardness value appeared in the heat affected zone. The order of microhardness values in the weld center from high to low was filling layer, backing layer, and covering layer; their microhardness values were 74 HV, 70 HV, and 67 HV, respectively. The average tensile strength of the joints reached up to 235.2 MPa, which was 79.7% of the base metal. The tensile specimen fractured near the fusion line in the heat affected zone and the fracture propagated approximately parallel to the fusion line, and the tensile fracture showed a typical plastic fracture mode. The median fatigue limit and safety fatigue limit of the welded joints were 99 MPa and 93 MPa, respectively. The fatigue specimen fractured in the weld metal, and the crack initiated in the backing layer.

**Keywords** Laser-MIG hybrid welding · Multi-layer welding · Medium-thick plate · Aluminum alloy · Microstructure · Mechanical properties

## 1 Introduction

With the demand of increasing in the running speed of the high-speed trains, aluminum alloys had been more and more adopted to manufacture train bodies due to their low density and high strength, especially the thin aluminum alloy extruded profiles [1, 2]. Considering the application advantages of the aluminum alloys, the medium-thick aluminum alloy plates and extruded profiles had been increasing applied in some important load-bearing components to further reduce the train weight and increase its running speed. However, current welding methods for thick plate aluminum

alloys faced challenges such as significant deformation, poor forming quality, and low efficiency [3, 4]. Therefore, it was becoming more necessary to develop a well-formed and efficient welding method for joining medium-thick aluminum alloy components.

At present, the metal inert-gas (MIG) welding and friction stir welding (FSW) are the most common welding methods for the medium-thick aluminum alloy components in the high-speed manufacturing industry. For the traditional MIG welding, the large groove angle and small blunt thickness were needed due to its weak penetration ability; subsequently, more welding layers and welding passes were required [5]. The above technological characteristics of the MIG welding determined that it had low production efficiency and high welding heat input, which ultimately caused large welding deformation and high residual stress as well as low mechanical properties [6, 7]. Therefore, for the welding of medium-thick aluminum alloys in the high-speed train manufacturing field, the MIG-welded components could no longer meet the requirements for the formation quality and

---

Recommended for publication by Commission IV - Power Beam Processes

✉ Zhibin Yang  
yangzhibin@djtu.edu.cn

<sup>1</sup> Dalian Jiaotong University, 794 Huanghe Road, Shahekou District, Dalian 116028, China

service safety [8]. Compared with the traditional MIG welding, friction stir welding had several obvious advantages of smaller welding deformation and higher mechanical properties due to the lower heat input [9]. Moreover, it could also realize single-layer welding for the medium-thick materials, the materials did not need to be machined to a certain groove which was very beneficial for reducing production costs. However, the widespread application of the friction stir welding had been significantly limited by the component structure and weld type, which nearly always applied in welding the long straight welds with rigid support on the backside [10]. In addition, the friction stir welding also demanded extremely high assembly accuracy, which presented a great challenge to the fixture used for practical production [11]. Therefore, it is urgent to propose a promising welding method to meet demands of well-formed and high-efficient joining for the medium-thick components in the high-speed trains manufacturing industry at the current period.

Laser-MIG hybrid welding combines the technical advantages of laser beam welding and MIG welding, had been applied in welding the thin aluminum alloy extruded profiles for the high-speed train bodies [12, 13]. Compared with the dominant MIG welding, the research and application results indicated that the laser-MIG hybrid welding had several distinct technical advantages such as higher welding speed, larger weld penetration, smaller heat input, lower welding deformation, and better mechanical properties [3, 14]. Numerous scholars had studied the welding characteristics of laser-MIG hybrid welding of thin aluminum alloy plates. Bunaziv et al. [15] pointed out that compared with arc in leading configuration, laser in leading configuration was beneficial to reduce the welding spatters due to it could improve the stability of the welding process. Huang et al. [16] demonstrated that the clockwise eddy in the lower molten zone had a lower flow velocity at a high welding speed, which was conducive to transfer the bubbles back into the keyhole and thus resulted in fewer pores. Zhao et al. [17] investigated the effects of the heat input on the weld quality of the laser-MIG hybrid welded aluminum alloy joints, the results indicated that higher MIG heat input was beneficial to reduce porosity defects and the reasonable energy ratio coefficient was 0.5. Huang et al. [18] studied the influence of the laser-wire distance on the weld formation, the results revealed that the laser-wire distance affected the energy distribution and droplet transition mode, and finally affected the weld penetration and formation.

Laser-MIG hybrid multi-layer welding method was generally adopted to joining the materials with the thickness over 15 mm, and the relevant researches were mainly focused on the steel materials at present. Zhan et al. [19] investigated the laser-MIG hybrid multi-layer welding for 19.5 mm thick Invar steel with different layer numbers, and demonstrated

that the weld surface of two-layer welding was better than that of three-layer welding, but the welding deformation and residual stress of three-layer were lower than those of two-layer welding due to the lower peak temperature in the three-layer welding. For 20-mm thick low carbon steel, Zhou et al. [20] obtained well-formed laser-MIG hybrid welded joints with few porosity defects and excellent mechanical properties by using three-layer welding method with the appropriate welding parameters. The groove shape was a crucial factor affecting the weld formation for the multi-layer welding. According to the research results of Wang et al. [21], the groove angle had an obvious effect on the weld inclination and molten weld metal flowing down, and the defect of incomplete fusion would appear when the groove angle was too small. Many scholars [22–25] had also found that the shape of the groove and the gap between the groups affected the arc shape during the welding process. The appropriate groove shape and the gap between the groups could enhance the stability of the arc during the welding process, which in turn affected the shape of the final weld. Meanwhile, the results of Çetkin et al. [26] indicated that the groove shape also had remarkable effects on the mechanical properties of the joints; the different groove shapes also had distinctly different fracture features. Huang et al. [27] pointed out that the blunt edge thickness of the groove obviously affected the weld formation, the weld surface was rough when the blunt edge thickness too small, and well-formed weld surface would be obtained when the blunt edge thickness increased to a certain extent. Based on the existing literatures review, it could find that there were very few reports focusing on the laser-MIG hybrid multi-layer welding for the medium-thick aluminum alloys.

Therefore, in the present work, laser-MIG hybrid multi-layer welding was performed upon the 20-mm thick 6082-T6 aluminum alloy butt-joints. The weld formation, microstructure, and mechanical properties of the welded joints were systematically investigated. The purpose of this research was to expand the application of the laser-MIG hybrid welding in high-speed train manufacturing industry for joining the medium-thick aluminum alloy components.

## 2 Materials and experimental procedures

### 2.1 Materials

The base metal used in the experiments was 6082-T6 aluminum alloy plate with a tensile strength of 295 MPa, whose size was 20 mm × 150 mm × 300 mm. Based on the numerous previous experimental results, a U-shape groove with the blunt edge thickness of 10 mm was machined as given in Fig. 1. Before welding, the base metal was preprocessed by mechanical grinding and scrubbing with acetone to

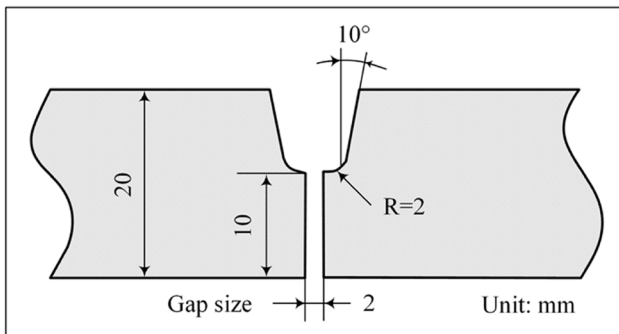


**Fig. 1** Dimensional diagram of the used U-shape groove

remove the oxide film and greasy dirt on its surface. The filler wire adopted in this work was ER5356 with a diameter of 1.2 mm. The chemical compositions of the base metal and filler wire are listed in Table 1.

### 2.2 Experimental apparatuses and methods

Laser-MIG hybrid welding experiments were carried out with a TRUMPF TruDisk 16,003 disk laser in combination with a FRONIUS TPS 5000 CMT welding machine, which were controlled by a KUKA 60 HA welding robot. The emission wavelength and focusing diameter of the laser were 1070 nm and 1.0 mm, respectively. The defocusing distance of the laser was 2 mm. During the welding process, the distance between the laser and filler wire was 3.0 mm, their inclination angles relative to the plate were 85° and 60°, respectively. The high purity argon (99.999%) adopted as the shielding gas with a flow rate of 35 L/min. Due to the

small surface tension of aluminum alloy, in order to prevent the backside of the weld from being too high, resulting in underfilling of the backing weld, the backside of the weld is forcibly shaped using an aluminum alloy pad. The schematic diagrams of the welding method and weld formation are presented in Fig. 2. In order to remove the impurities and contaminants existed on the surfaces of the interlayers, the interlayer cleaning was carried out by mechanical grinding. Based on the numerous previous experimental results, three-layer welding method was determined, which consisted of backing welding, filling welding, and covering welding. The optimal laser-MIG hybrid welding parameters for each layer adopted in this work are given in Table 2. The temperature between layers was controlled no more than 120 °C.

Referring to ISO 17636–1: 2013, the porosity defects in the weld seams were detected by an XXG-2005 X-ray testing equipment. The macroscopic features and microstructures of the weld cross-sections were observed by an Olympus BX 51 M metallographic microscope. According to GB/T 2654–2008, the microhardness testing was carried out on the weld cross-section using a FM-700 microhardness tester with a load of 100 g for 15 s. Referring to GB/T 2651–2008, the tensile testing was executed by a WDW-300E electronic universal testing machine, and the loading speed was 2 mm/s, and the average of 3 pieces of test was taken as the final result. According to Q/SF 55–020-2009, the fatigue testing employed group method and up-down method was conducted by a QBG-200 high-frequency fatigue testing machine, and the cyclic stress ratio was 0. The schematic diagrams of the tensile and fatigue testing specimens are shown in Fig. 3, and their weld reinforcements had been removed and polished. The fracture features of the tensile

**Table 1** Chemical compositions of the base metal and filler wire (wt. %)

Materials	Si	Fe	Cu	Mn	Mg	Cr	Zn	Ti	Al
AA6082-T6	0.97	0.37	0.07	0.67	1.02	0.01	0.06	0.01	Bal.
ER5356	0.10	0.4	0.1	0.15	4.8	0.1	0.1	0.13	Bal.

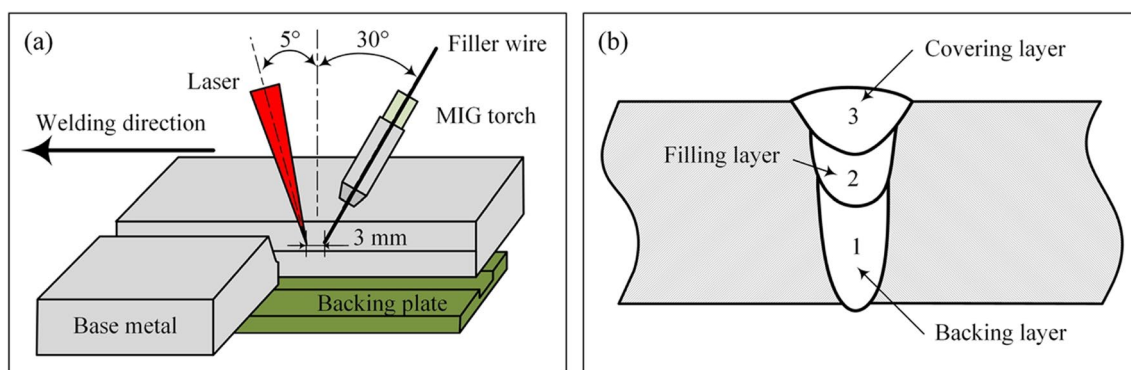


**Fig. 2** Schematic diagrams of the laser-MIG hybrid welding: **a** welding method; **b** weld formation

and fatigue testing specimens were observed by a SUPRA 55 scanning electron microscope.

### 3 Results and discussion

#### 3.1 Weld formation

Based on the corresponding optimal laser-MIG hybrid welding parameters, the weld cross-sections, surface formations, and porosity defects of the different layers are presented in Fig. 4. The results indicated that the well-formed weld formation could be obtained by using three-layer welding method. The weld penetrations of the backing layer, filling layer, and covering layer were 12.8 mm, 5.8 mm, and 7.0 mm, respectively, and the weld widths were 9.5 mm,

8.1 mm, and 13.8 mm, respectively. No obvious welding defects such as incomplete fusion, cracks, and porosities were observed on the weld cross-sections of each layer. Meanwhile, there were also no visible porosities, cracks, and other forming defects could be found on the weld surfaces. The X-ray testing results indicated that no porosity defects existed in weld seam of the backing layer, as shown in Fig. 4a. By comparison, there were very few small size porosities could be observed in the weld seam of filling layer and covering layer, as shown in Fig. 4b and c. The keyhole was a through passage during the backing welding process, which was beneficial for the pores to escape from the weld molten pool via it [28]. For the filling welding and covering welding process, the pores could no longer escape from the bottom of the keyhole, which would lead to an increased probability of the porosity formation.

**Table 2** The optimal laser-MIG hybrid welding parameters for each layer adopted in this work

Layers	Welding speed $V/m/min$	Laser power $P/kW$	Arc current $I/A$	Arc voltage $U/V$	Wire feeding speed $V_f/m/min$	Arclength correction $\eta/\%$	Linear energy $q/kJ/cm$	Arc energy rate $\phi/\%$
Backing layer	0.6	6.5	300	25.0	17.5	-5	10.72	45.3
Filling layer	0.7	3.5	280	24.7	16.8	-5	6.55	58.8
Covering layer	0.6	2.5	300	27.6	17.5	+5	7.63	70.5

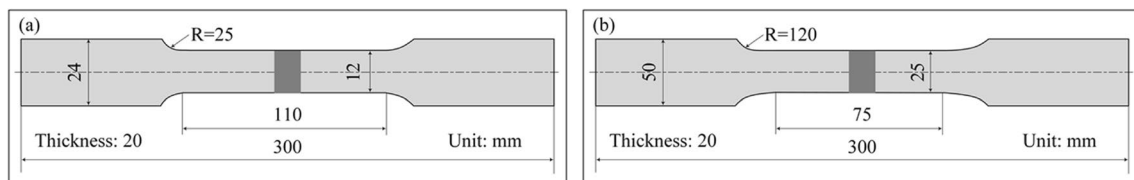
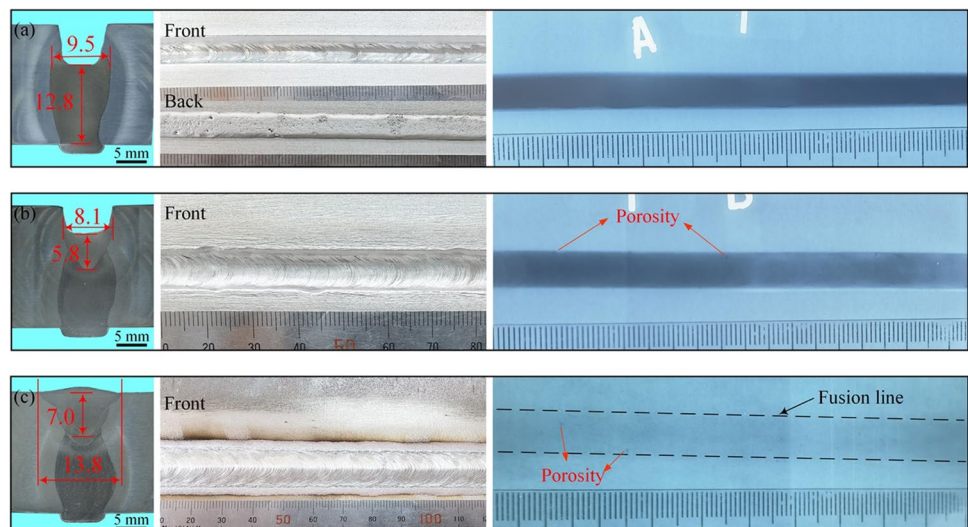


**Fig. 3** Schematic diagrams of the specimens: **a** for tensile testing; **b** for fatigue testing

**Fig. 4** Weld cross-sections, surface formations, and porosity defects of the different layers: **a** backing layer; **b** filling layer; **c** covering layer



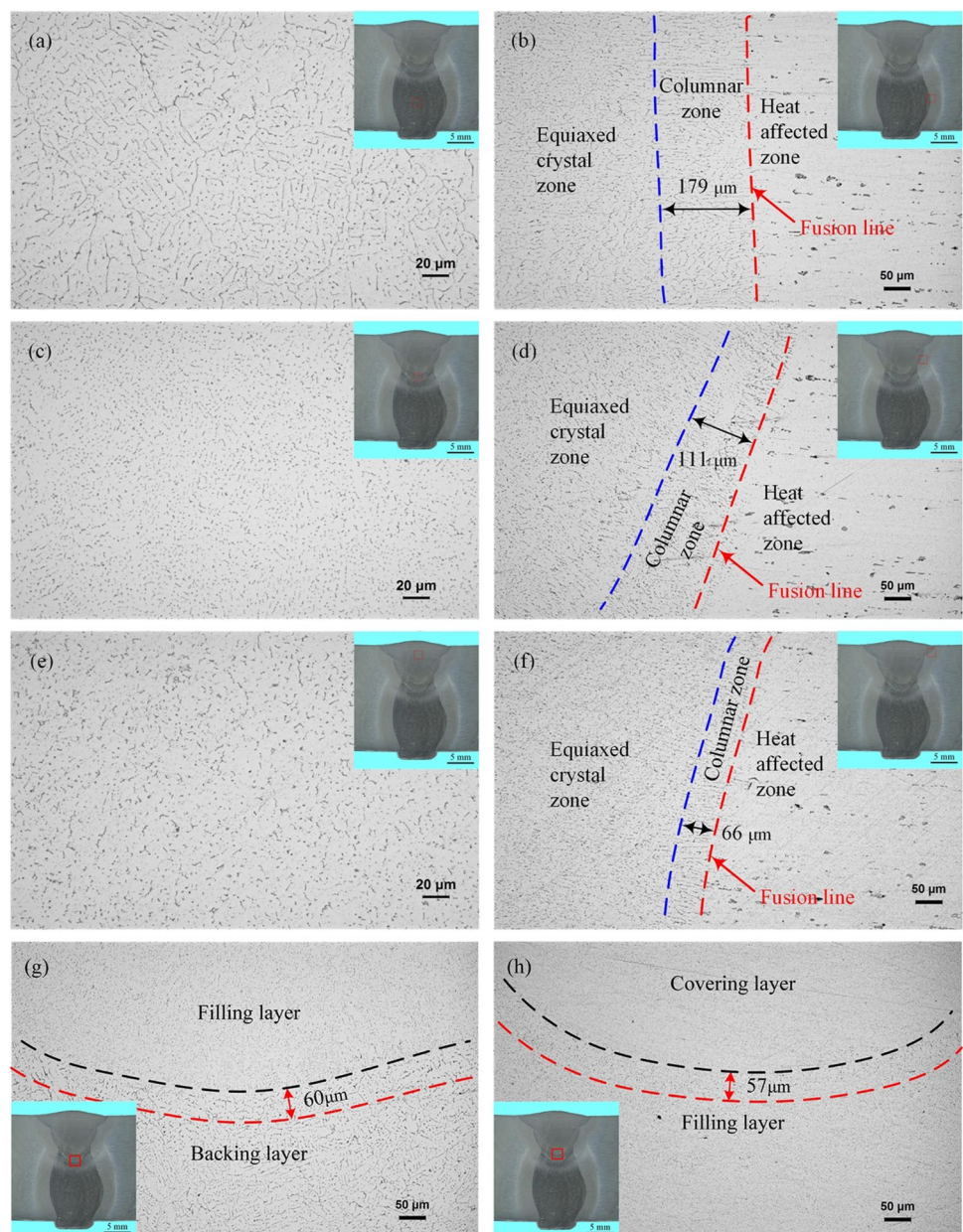


### 3.2 Microstructures

The microstructures in the weld center and heat affected zone of each layer are shown in Fig. 5. The equiaxed crystals could be observed in the weld center of each layer, as shown in Fig. 5a, c and e. The difference was that the equiaxed crystal size of the backing layer was the largest due to it had highest linear energy, and that of the filling layer was the smallest because of its lowest linear energy. The welding heat input of the backing layer (10.72 kJ/cm) was greater than the welding heat input of the covering layer (7.63 kJ/cm) and the filling layer (6.55 kJ/cm). The larger the heat input, the larger the equiaxed crystal size. The distinct columnar crystals could be found near the fusion in the weld

metal of each layer. The columnar zone widths of the backing layer, filling layer, and covering layer were respectively about 179  $\mu\text{m}$ , 111  $\mu\text{m}$ , and 66  $\mu\text{m}$ , as shown in Fig. 5b, d and f. The different cooling rate was the main reason for this difference: the larger cooling rate, the wider the columnar zone width [29]. During the backing welding process, the base metal directly connect with the fixture was beneficial to rapidly reduce the temperature of the weld molten pool and finally obtain the widest columnar zone. For each layer, there was no obvious grain coarsening in the heat-affected zone. The microstructures near the interlayers indicated that there were no visible defects, as shown in Fig. 5g and h. The results also indicated that the subsequent welding did not have obvious influence on the microstructures of the former

**Fig. 5** Microstructures of the laser-MIG hybrid multi-layer welded joints: **a** in weld center of backing layer; **b** near fusion line of backing layer; **c** in weld center of filling layer; **d** near fusion line of filling layer; **e** in weld center of covering layer; **f** near fusion line of covering layer; **g** interlayer between backing layer and filling layer; **h** interlayer between filling layer and covering layer



weld; only the crystal size grew slightly in the range of about 60  $\mu\text{m}$  near the former weld interlayers.

### 3.3 Microhardness distribution

The microhardness distributions of the laser-MIG hybrid multi-layer welded joint are shown in Fig. 6. Compared with the microhardness values of the base metal, those of the weld metal and heat-affected zone obviously decreased in each layer, and the lowest microhardness value existed in the heat-affected zone, as shown in Fig. 6a, b and c, which indicated that the softening phenomenon occurred for the laser-MIG hybrid multi-layer welded joints. The vaporization of alloying elements was recognized as the main reason for the decrease of the microhardness in the weld metal [30, 31]. Meanwhile, the grain size difference in the weld metal and base metal was another reason for the difference in microhardness in the above regions. The microhardness decreased in the heat-affected zone was caused by the alloying elements diffused toward to the weld molten pool [32]. The microhardness values in the weld center of different layers were different: filling layer was the highest, backing layer was the middle, and covering layer was the lowest; their microhardness values were 74 HV, 70 HV, and 67 HV, respectively, as shown in Fig. 6d.

The difference in the microhardness values of each layer was mainly attributed to the comprehensive effects of heat

input, cooling rate, and high temperature residence time. Compared with the microhardness value of filling layer, that in the weld metal of backing layer was lower mainly due to more alloying elements vaporized caused by the higher heat input, and that in the heat-affected zone of backing layer decreased less significantly due to fewer alloying elements diffused toward to the weld molten pool caused by the larger cooling rate. However, compared with the microhardness value of filling layer and backing layer, the longest high temperature residence time of the covering layer was the dominant reason for its lowest microhardness value. For the covering layer, compared with the microhardness value in the weld metal, there was hardly any reduction in the heat-affected zone except near the fusion line, which might be related to the excessive proportion of arc energy in the heat source.

### 3.4 Tensile properties

The tensile testing results of the laser-MIG hybrid multi-layer welded joints are given in Table 3. The average tensile strength and average elongation of the laser-MIG hybrid multi-layer welded joints reached up to 235.2 MPa and 6.2%, which were 79.7% and 77.5% of the base metal, respectively. The tensile curve of the laser-MIG hybrid multi-layer welded joints as shown in Fig. 7.

**Fig. 6** Microhardness distributions of the laser-MIG hybrid multi-layer welded joint: **a** backing layer; **b** filling layer; **c** covering layer; **d** along thickness direction

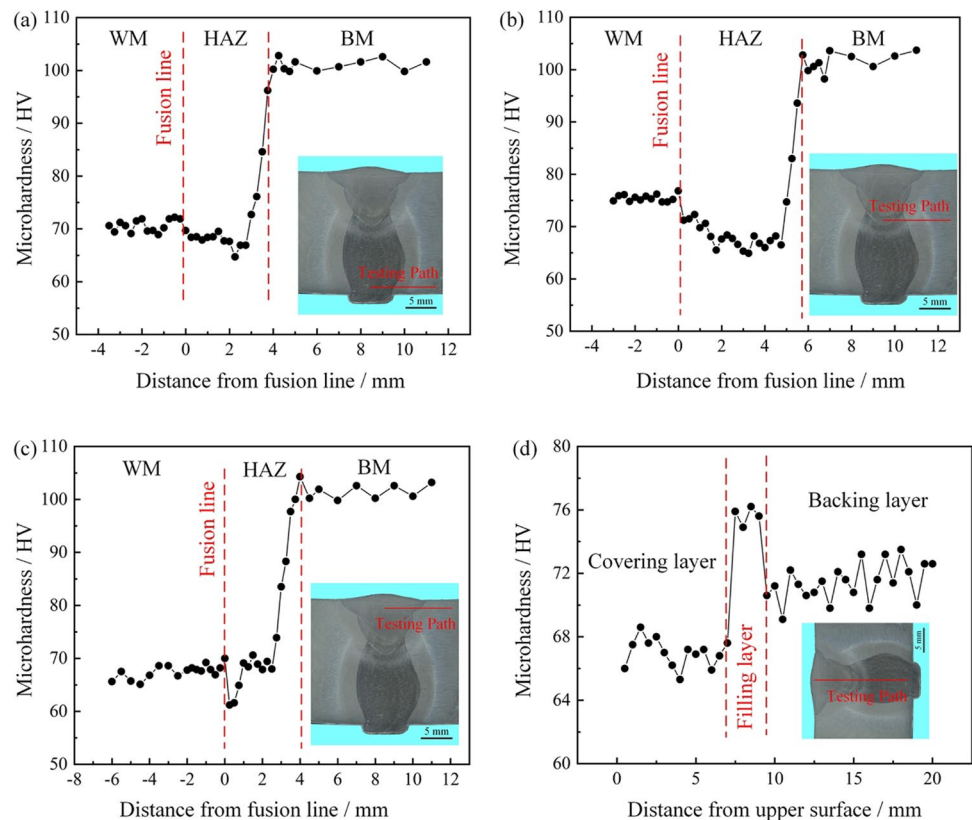




**Table 3** Tensile testing results of the laser-MIG hybrid multi-layer welded joints

No	Tensile strength $R_m$ /MPa		Joint efficiency $\chi$ /%	Elongation $A$ /%		Fracture location
	Single	Average		Single	Average	
LS-1#	234.9	235.2	79.7	6.7	6.2	Near fusion line
LS-2#	236.5			6.3		Near fusion line
LS-3#	234.1			5.7		Near fusion line

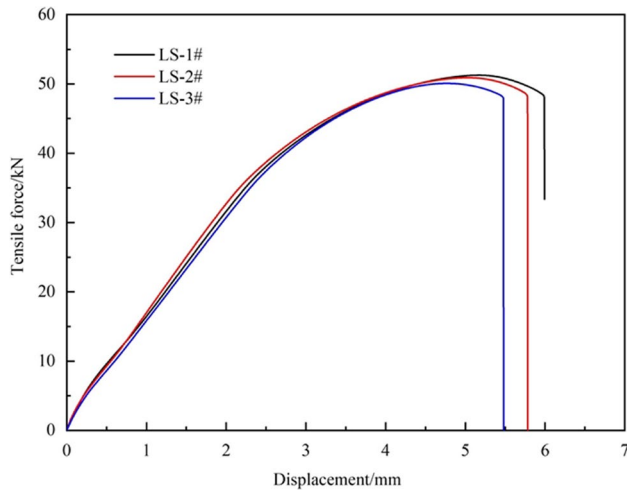


**Fig. 7** The tensile curve of the laser-MIG hybrid multi-layer welded joint

The tensile testing specimens all fractured in near the fusion line in the heat-affected zone. The fracture locations and macroscopic and microscopic features of the tensile

testing specimen are provided in Fig. 8. The tensile testing specimen fracture occurred near the fusion line in the heat-affected zone due to the lowest microhardness value existed near the fusion line in the covering layer, and the fracture propagated approximately parallel to the fusion line, as shown in Fig. 8a and b. The results indicated that the above region was the weakest area of the laser-MIG hybrid multi-layer welded joint. There were no visible defects such as porosity, cracks, and incomplete fusion could be observed on the macroscopic fracture, as shown in Fig. 8c. Lots of distinct dimples could be found on the microscopic fractures of the backing layer, filling layer, and covering layer, as shown in Fig. 8d, e and f. It revealed that the fracture was showing a feature of plastic fracture.

### 3.5 Fatigue properties

Based on the results obtained by group and up-down fatigue tests, the  $S-N$  fatigue curve of the laser-MIG hybrid multi-layer welded joints is presented in Fig. 9. The median fatigue limit with 50% survival rate was 99 MPa, the safety fatigue limit with 80% survival rate and 95% confidence coefficient

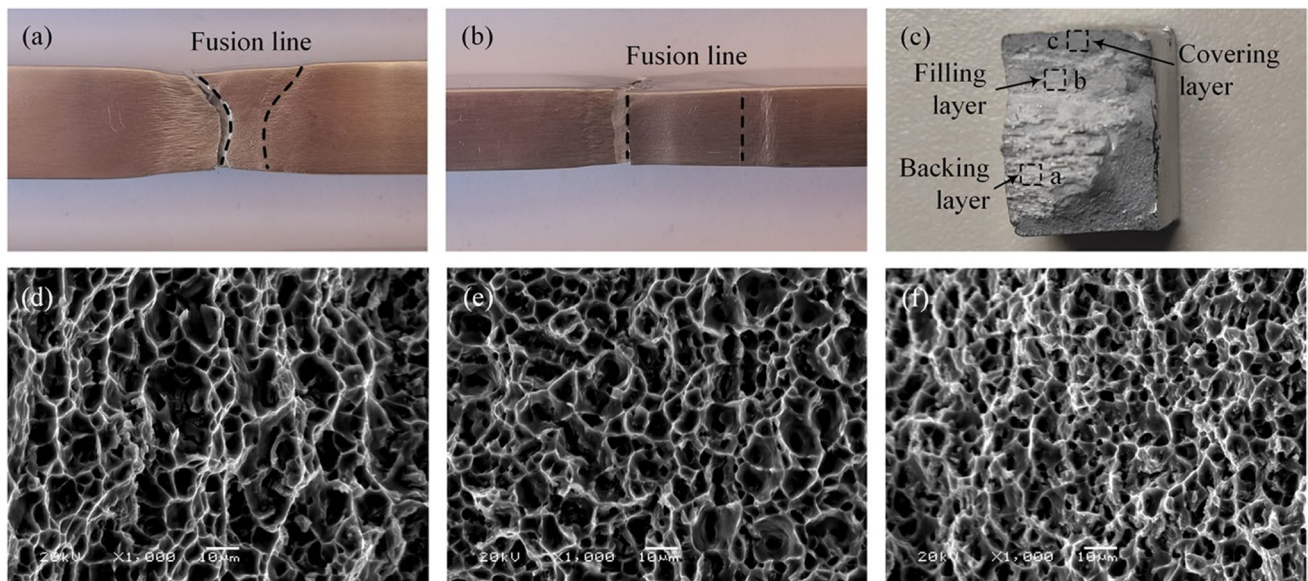


**Fig. 8** Fracture features of the tensile specimen: **a** fracture location along thickness direction; **b** fracture location on weld surface; **c** macroscopic fracture; **d** microscopic fracture on backing layer; **e** microscopic fracture on filling layer; **f** microscopic fracture on covering layer

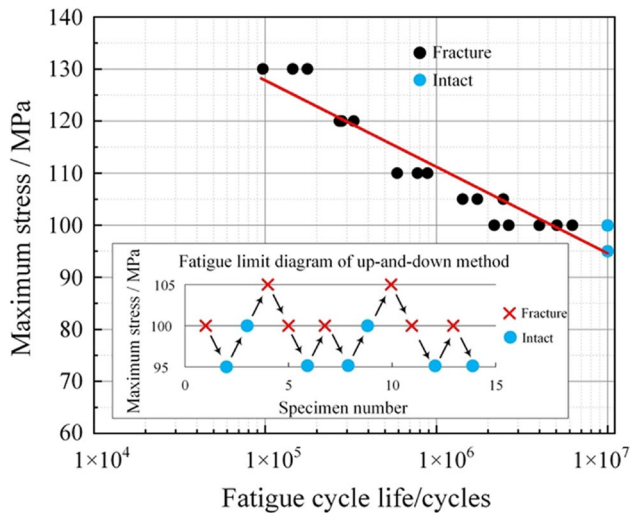


**Fig. 9** *S*–*N* fatigue curve of the laser-MIG hybrid multi-layer welded joints

was 93 MPa. The fracture locations and macroscopic and microscopic features of the fatigue testing specimen are shown in Fig. 10. The fatigue specimen fractured in the weld metal, and the crack initiated in the backing layer, as shown in Fig. 10a. The macroscopic fracture surface consisted of three distinct different regions, including crack initiation region, crack propagation region, and final fracture region,

as shown in Fig. 10b. There was a welding defect of elongated cavity found in the crack initiation region, as shown in Fig. 10c, which caused serious stress concentration and finally resulted in the crack initiated [33]. Obvious fatigue striations could be observed in the crack propagation region, as shown in Fig. 10d. In the final fracture region, its fracture feature was similar to that of the tensile specimen except for existing several secondary cracks, as shown in Fig. 10e.

## 4 Conclusions

- For 20-mm thick aluminum alloy butt-joint, the well-formed weld could be obtained by using the laser-MIG hybrid three-layer welding method. There were no obvious incomplete fusion and cracks observed in each layer, and very few porosity defects appeared in the filling layer and covering layer.
- The equiaxed crystals and columnar crystals were respectively observed in the weld center and near the fusion in the weld metal of each layer; their sizes and widths were different due to the different heat inputs, cooling rates, and high temperature residence times. The subsequent welding did not have obvious influence on the microstructures of the former weld.
- The microhardness values of the weld metal and heat-affected zone lower than those of the base metal, the

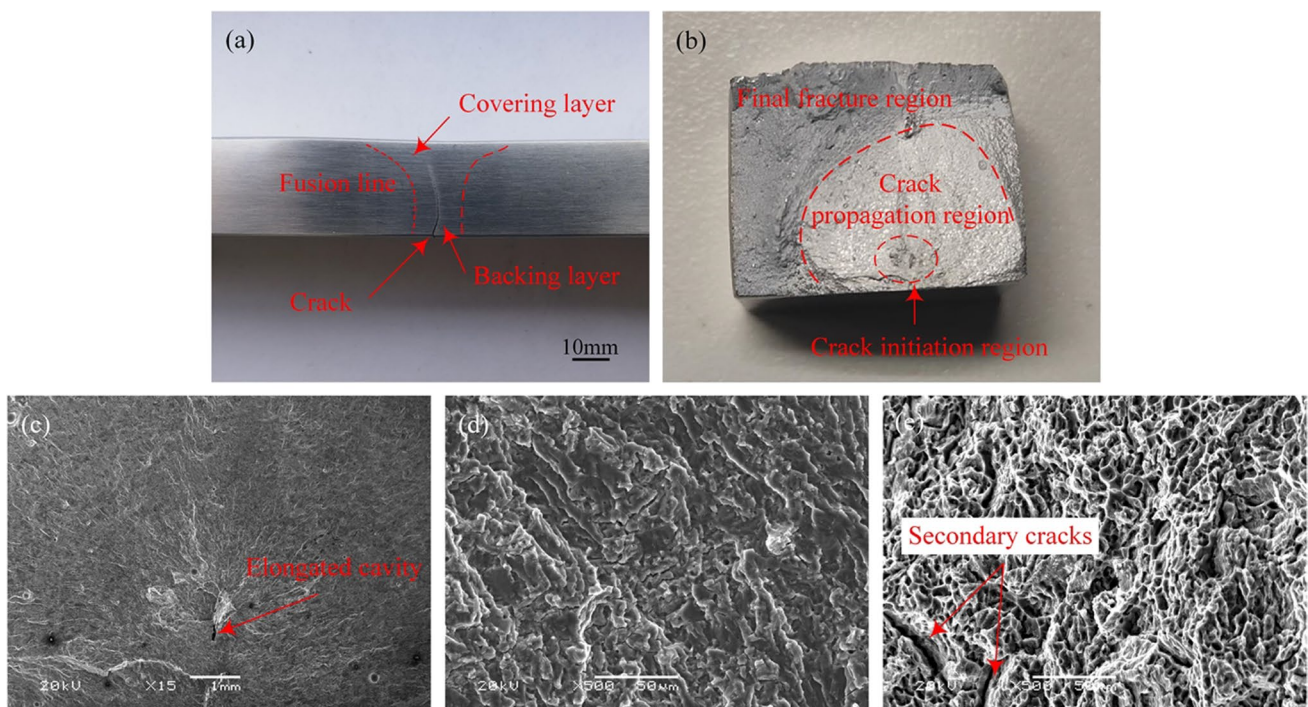


**Fig. 10** Fracture features of the fatigue specimen: **a** fracture location; **b** macroscopic fracture; **c** microscopic fracture in crack initiation region; **d** microscopic fracture in crack propagation region; **e** microscopic fracture in final fracture region



lowest microhardness value appeared in the heat-affected zone. The order of microhardness values in the weld center of each layer from high to low was filling layer, backing layer, and covering layer.

- The average tensile strength of the laser-MIG hybrid multi-layer welded joints reached up to 235.2 MPa, which was 79.7% of the base metal. The tensile specimen fractured near the fusion line in the heat-affected zone and the fracture propagated approximately parallel to the fusion line. The tensile fracture showed a typical plastic fracture mode.
- The median fatigue limit and safety fatigue limit of the laser-MIG hybrid multi-layer welded joints were 99 MPa and 93 MPa, respectively. The fatigue specimen fractured in the weld metal, and the crack initiated in the backing layer. Obvious fatigue striations could be observed in the crack propagation region.

**Author contribution** All authors contributed to the study conception and design. Material preparation, data collection, and analysis were performed by Zhibin Yang, Likang Sheng, and Yanqi Xie. The first draft of the manuscript was written by Zhibin Yang and all authors commented on previous versions of the manuscript. All authors read and approved the final manuscript.

**Funding** The research was supported by the Liaoning Provincial Education Department Scientific Research Foundation of China [grant number JDL2020026].

**Data availability** The data supporting the findings of this study are available within the article.

## Declarations

**Competing interests** The authors declare no competing interests.

## References

- Gou G, Zhang M, Chen H et al (2015) Effect of humidity on porosity, microstructure, and fatigue strength of A7N01S-T5 aluminum alloy welded joints in high-speed trains. *Mater Des* 85:309–317
- Xin Z, Yang Z, Zhao H et al (2019) Comparative study on welding characteristics of laser-CMT and plasma-CMT hybrid welded AA6082-T6 aluminum alloy butt joints. *Materials* 12:3300
- Jiang Z, Hua X, Huang L et al (2018) Double-sided hybrid laser-MIG welding plus MIG welding of 30-mm-thick aluminium alloy. *Int J Adv Manuf Technol* 97:903–913
- Huang L, Hua X, Wu D et al (2019) A study on the metallurgical and mechanical properties of a GMAW-welded Al-Mg alloy with different plate thicknesses. *J Manuf Process* 37:438–445
- Wang T, Li Y, Mao Y et al (2022) Research status of deep penetration welding of medium-thick plate aluminum alloy. *Int J Adv Manuf Technol* 120:6993–7010
- Cornacchia G, Cecchel S, Panvini A (2018) A comparative study of mechanical properties of metal inert gas (MIG)-cold metal transfer (CMT) and fiber laser-MIG hybrid welds for 6005A T6 extruded sheet. *Int J Adv Manuf Technol* 94:2017–2030
- Chen L, Mi G, Zhang X et al (2019) Numerical and experimental investigation on microstructure and residual stress of multi-pass hybrid laser-arc welded 316L steel. *Mater Des* 168:107653
- Du L, Yang Z, Wang X (2023) Welding characteristics of laser-MIG hybrid welding of arc-welded aluminum profiles for high-speed trains. *Materials* 16:404
- Chumaevsii A, Amirov A, Ivanov A et al (2023) Friction stir welding / processing of various metals with working tools of different materials and its peculiarities for titanium alloys: A review. *Metals* 13:970
- Kulekci MK, Esme U, Buldum B (2016) Critical analysis of friction stir-based manufacturing processes. *Int J Adv Manuf Technol* 85:1687–1712
- Padhy GK, Wu CS, Gao S (2018) Friction stir based welding and processing technologies - processes, parameters, microstructures and applications: A review. *J Mater Sci Technol* 34:1–38
- Wang Q, Chen H, Zhu Z et al (2016) A characterization of microstructure and mechanical properties of A6N01S-T5 aluminum alloy hybrid fiber laser-MIG welded joint. *Int J Adv Manuf Technol* 86:1375–1384
- Han X, Yang Z, Ma Y et al (2023) Laser-MIG hybrid welding of aluminum alloy extrusions for high-speed trains: effects of gap width on microstructure and properties. *Weld Int* 37:334–343
- Fan C, Yang S, Zhu M et al (2021) Microstructure and fatigue properties of 6061 aluminum alloy laser-MIG hybrid welding joint. *Adv Mater Sci Eng* 2:1–12
- Bunaziv I, Akselsen OM, Salminen A et al (2016) Fiber laser-MIG hybrid welding of 5 mm 5083 aluminum alloy. *J Mater Process Tech* 233:107–114
- Huang S, Xu L, Lou M et al (2023) Keyhole-induced pore formation mechanism in laser-MIG hybrid welding of aluminum alloy based on experiment and multiphase numerical model. *J Mater Process Tech* 314:117903
- Zhao Y, Zhan X, Zhou X et al (2021) Effect of heat input on macro morphology and porosity of laser-MIG hybrid welded joint for 5A06 aluminum alloy. *Int J Adv Manuf Technol* 115:4035–4045
- Huang H, Zhang P, Yan H et al (2021) Research on weld formation mechanism of laser-MIG arc hybrid welding with butt gap. *Opt Laser Technol* 133:106530
- Zhan X, Liu Y, Ou W et al (2015) The numerical and experimental investigation of the multi-layer laser-MIG hybrid welding for Fe36Ni invar alloy. *J Mater Eng Perform* 24:4948–4957
- Zhou S, Ling W, Ma W et al (2019) The pores formation mechanism in the laser-MIG hybrid welded joint of mild steel. *Mater Res Express* 6:095803
- Wang K, Jiao X, Zhu J et al (2021) Research on the effect of weld groove on the quality and stability of laser-MAG hybrid welding in horizontal position. *Weld World* 65:1701–1709
- Zhu C, Tang X, He Y et al (2023) Study on arc characteristics and their influences on weld bead geometry in narrow gap GMAW of 5083 Al-alloy. *Int J Adv Manuf Technol* 90(9–12):2513–2525
- Yu J, Cai C, Xie J et al (2023) Weld formation, arc behavior, and droplet transfer in narrow-gap laser-arc hybrid welding of titanium alloy. *J Manuf Process* 91:44–52
- Zhao Y, Zhou X, Liu T et al (2020) Investigate on the porosity morphology and formation mechanism in laser-MIG hybrid welded joint for 5A06 aluminum alloy with Y-shaped groove. *J Manuf Process* 57:847–856
- Yu J, Cai C, Xie J et al (2024) Keyhole stability, arc behavior, and molten pool flow in narrow-gap oscillating laser-arc hybrid welding of titanium alloy. *Int J Heat Mass Tran* 97:44–52

26. Çetkin E, Çelik YH, Temiz Ş (2020) Effect of welding parameters on microstructure and mechanical properties of AA7075/AA5182 alloys joined by TIG and MIG welding methods. *J Braz Soc Mech Sci Eng* 42:34
27. Huang A, Zhang J, Gao C et al (2019) Effects of groove constraint space on plasma characteristics during Laser-MIG hybrid welding of Titanium alloy. *J Manuf Process* 48:137–144
28. Yang Z, Zhao X, Tao W et al (2019) Effects of keyhole status on melt flow and flow-induced porosity formation during double-sided laser welding of AA6056/AA6156 aluminium alloy T-joint. *Opt Laser Technol* 109:39–48
29. David SA, Vitek JM (1989) Correlation between solidification parameters and weld microstructures. *Int Mater Rev* 34:213–245
30. Liu S, Li J, Mi G et al (2016) Study on laser-MIG hybrid welding characteristics of A7N01-T6 aluminum alloy. *Int J Adv Manuf Technol* 87:1135–1144
31. Beiranvand ZM, Ghaini FM, Moosavy HN et al (2020) The relation between magnesium evaporation and laser absorption and weld penetration in pulsed laser welding of aluminum alloys: Experimental and numerical investigations. *Opt Laser Technol* 128:106170
32. Zhang X, Li L, Chen Y et al (2017) Effects of pulse parameters on weld microstructure and mechanical properties of extra pulse current aided laser welded 2219 aluminum alloy joints. *Materials* 10:1091
33. Sepe R, Wiebesiek J, Sonsino CM (2020) Numerical and experimental validation of residual stresses of laser-welded joints and their influence on the fatigue behavior. *Fatigue Fract Eng Mater Struct* 43:1126–1141

**Publisher's Note** Springer Nature remains neutral with regard to jurisdictional claims in published maps and institutional affiliations.

Springer Nature or its licensor (e.g. a society or other partner) holds exclusive rights to this article under a publishing agreement with the author(s) or other rightsholder(s); author self-archiving of the accepted manuscript version of this article is solely governed by the terms of such publishing agreement and applicable law.